Microalgae-derived cellulose/inorganic nanocomposite rattle-type microspheres as an advanced sensor for pollutant detection

Lei Bi[a], Yi-Ping Chen*[b], [c], Chen Wang[a], Jing Su[a] and Gang Pan*[a], [d], [e]

[a] Dr. L. Bi, Dr. C. Wang, Dr. J. Su, Prof. G. Pan

Key Laboratory of Environmental Nanotechnology and Health Effects, Research Center for Eco-Environmental Sciences, Chinese Academy of Sciences, Beijing 100085, China

E-mail: gpan@rcees.ac.cn

[b] Prof. Y. P. Chen

College of Food Science and Technology, Huazhong Agricultural University, Wuhan, 430070, China

E-mail: chenyiping@mail.hzau.edu.cn

[c] Key Laboratory of Environment Correlative Dietology, Huazhong Agricultural University, Ministry of Education, Wuhan, China

[d] Centre of Integrated Water-Energy-Food studies (iWEF), School of Animal, Rural and Environmental Sciences, Nottingham Trent University, Brackenhurst Campus, Southwell, NG25 0QF, U.K.

[e] Beijing Advance Sciences and Innovation Center, Chinese Academy of Sciences, Beijing, China

Abstract

The versatility of rattle-type microspheres is tightly correlated with the composition and morphology. Exploring advanced rattle-type microspheres with simultaneous controllable composition and micro/nanostructures via novel designed and regulated strategies may have great advantages for performing complex tasks. Herein, cellulose/inorganic hybrid rattle-type microspheres, produced using microalgae as natural chemical reservoirs, microreactors and matrix, is reported. By adjusting only pH and temperature, rattle-type microspheres with simultaneously controllable mesoporous outer shells (19.4 to 46.3 nm) and multicomponent nanocores (i.e., $Ca_5(PO_4)_3OH$ and $Fe_3O_4/MgFe_2O_4$) are obtained using microalgae as single-source precursors. Especially, the rattle-type microspheres-mediated immunosensor shows ultrahigh sensitivity for the detection of trace microcystin-LR in complex real water samples with a limit of quantitation of 0.05 ng/mL, which is a 10-fold improvement compared with conventional enzyme linked immunosorbent assays. Enhancement of the sensitivity is due to the tailorability and functionality in both the hollow shells and the cores of the rattle-type microspheres. The finely controlled pore-size, void space and natural carboxyl groups of the shell are beneficial for enzymes loading and for bio-conjugation. The cores contain magnetite and hydroxyapatite nano-particles, which can be utilised for magnetic separation and for anchoring more enzymes, resulting in considerable signal amplification. This work opens up a new and green route for the construction of rattle-type microspheres with tunable compositions and porosities, which makes it a flexible platform for various applications in immunoassay,

biosensors, enrichment and separation of target substances, drug-delivery, and environmental remediation.

Keywords

Hollow materials; porous materials; microspheres; core-shell structure; green synthesis; immunoassay.

1. Introduction

Rattle-type structured microspheres are a type of core-shell structure with one or more movable cores, and which have received considerable attention in recent years, having been utilised in a wide range of applications as micro-reactors [1], drug delivery agents [2-4], tumor therapy [5, 6], adsorbent [7, 8], catalysis [9-12], microwave absorption [13], and energy storage [14-16]. The performance of these versatile rattle-type materials is tightly correlated with the core components, the interior space, and the shell structures [17]. Therefore, it becomes an important research direction on the construction of rattle-type materials with multiple compositions and controllable morphology, which are capable of performing multiple tasks that cannot be obtained in single-component/geometry rattle-type materials [18, 19]. However, the fabrication of rattle-type materials, with simultaneous controllable multicomponent cores and pore-size shells, remains a significant challenge [20-23]. Particularly, the fabrication of complicated rattle-type materials commonly involves cumbersome processes using relatively expensive and potentially harmful man-made chemical precursors [20]. Therefore, synthesis of rattle-type materials with controllable compositions and morphology using environmentally friendly precursors and readily adjustable

technique is an idea worth investigating.

Recently, intensive attention has been paid to the synthesis of multifunctional micro/nanostructure materials using bio-sourced materials due to their natural micro/nano-structures, ready availablility and environment-friendly features [24-36]. As one of the most widespread existence of biotic resources, the cell of a green algae can be considered as a natural core-shell structured microsphere composed of protoplast as the inner core and tough cell wall as the outer shell. The protoplast can be considered as natural chemical reservoir which is full of chemical elements. Presuming that the natural elements inside the protoplast of microalgae can be converted into multicomponent cores with the cell wall acting as a micro-reactor and a matrix, the cell of green algae will transform from core−shell to rattle-type structured microsphere with multicomponent cores. Thus, it would be highly advantageous, for the preparation of sustainable and green multiple functional rattle-type microspheres, to utilize microalgae as single-source precursors.

Microcystin (MC) contamination has become a worldwide concern due to the increased occurrence of cyanobacteria blooms in surface waters that are used for drinking water supplies. One of the most toxic and widespread MCs is microcystin-LR (MC-LR), accounting for 46.0–99.8% of the total MCs in cyanobacterial blooms [37]. A convenient and highly efficient method for the detection of MC-LR is thus necessary to guarantee drinking water safety. Conventional enzyme linked immunosorbent assay (ELISA) is a widely used immunoassay for detection of MC-LR [38]. However, ELISA needs an

89 enzyme-labeled antibody conjugate, and one antibody molecule usually conjugates
90 with only one or two enzyme molecules covalently, which limits its sensitivity. Many
91 efforts have been made to solve this problem. One effective strategy is the preparation
92 of an enzyme cluster in order to increase the sensitivity of the immunoassay [39].
93 Another way is to fabricate magnetic nanoparticles (MNP) as magnetic separation
94 carriers to conjugate massive enzyme molecules and enrich targets from complex
95 samples for improving the sensitivity of the analysis [40, 41]. However, these
96 strategies need to utilize covalent conjugation, which in turn will affect the activity of
97 the enzyme, and furthermore, these MNPs are produced from man-made chemical
98 precursors that need complex surface functionalization in order to meet the
99 requirements of immunoassay [42]. For these reasons, exploring a novel material via a
100 'green' synthetic strategy that, due to the tailorability and functionality in both the
101 cores and hollow shells of rattle-type microspheres [43], can not only load large
102 amounts of enzyme and retain its activity without covalent conjugation, but can also
103 achieve magnetic separation and bioconjugation with antibodies without extra surface
104 functionalization, has the potential to improve the sensitivity and simplify
105 conventional ELISA.

106 In this study, we present a novel synthesis strategy by using microalgae as natural
107 chemical reservoir, microreactor and matrix for fabricating rattle-type microspheres
108 with simultaneous controllable multicomponent cores and pore-size shells (**Scheme 1**).
109 Its advantages are many-fold. The protoplast of the microalgae acts as a natural
110 chemical reservoir of Ca, Mg, P, and Fe for the formation of the multicomponent

inner cores, and the cell wall acts as a microreactor and a matrix to provide confined-space for the synthesis of inner cores and form the porous outer shell. By adjustment of only the initial pH and temperature of the hydrothermal reaction, rattle-type microspheres with simultaneous controllable multicomponent nano-cores and pore-size shell can be obtained. In particular, we have found that the microalgae-derived rattle-type microspheres were ideal signal multipliers for the development of a highly sensitive immunoassay, where the sensitivity of the immunoassay had been improved by an order of magnitude compared to that of conventional ELISA.

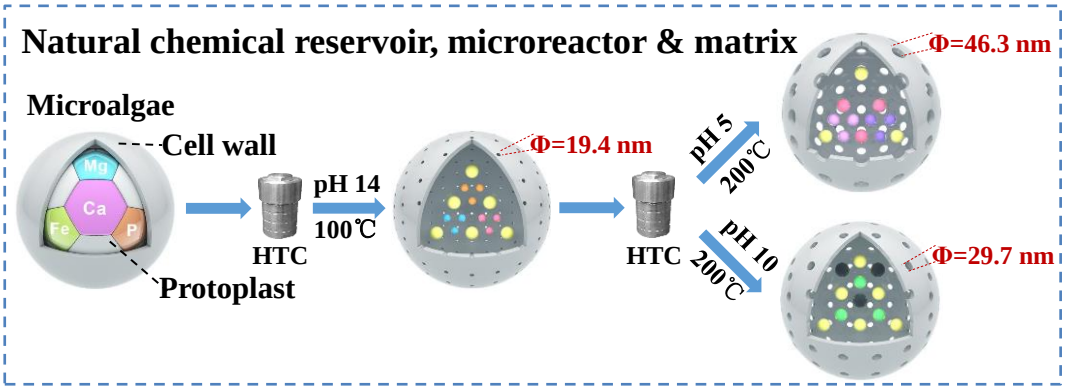

Scheme 1. Schematic of pH-/thermo induced synthesis of rattle-type microspheres with simultaneous controllable pore-size shell and multicomponent cores using microalgae as single-source precursors.

2. Experimental

2.1 Preparation of rattle-type microspheres

For the fabrication of microspheres (pH 14, 100 °C), 2 g *Chlorella pyrenoidosa* powder was added in 1% sodium dodecyl sulfate (SDS) solution and treated ultrasonically (100 W) for about 0.5 h in order to fully disperse the microalgal

aggregates, washed 5 times with deionized water to removal the SDS, dispersed in 40 mL NaOH solution (pH 14) and stirred intensely at 100 °C for 2 h. After reaction, the solid products were recovered by centrifugation and washed with abundant deionized water until the pH was neutral.

For the fabrication of microspheres (pH 10, 200 °C) and microspheres (pH 5, 200 °C), 0.5 g wet solid product of microspheres (pH 14, 100 °C) were dispersed in 40 mL deionized water and the pH appropriately adjusted to 10 or 5 with 0.1 mol/L NaOH or HCl, and then transferred to a 50 mL Teflon-sealed autoclave. The autoclave was transferred into a muffle furnace which had been preheated to 200 °C and maintained at this temperature for 4 h. Afterwards the autoclave was removed from the muffle furnace and cooled to ambient temperature, the solid products centrifuged and washed several times until the pH was neutral. An aliquot of the wet solid was freeze-dried for further analysis.

2.2 Preparation of horseradish peroxidase (HRP)@Microspheres@Antibody(Ab)-mediated ELISA (MPs-ELISA) conjugation

1000 μL of 5 mg/mL microspheres (pH 10, 200 °C) were magnetically separated and re-dispersed using 200 μL of PBS solution (pH=7.4, 0.01 M). 2 mg of HRP were added to this microspheres solution, and the mixture shaken for 2 h. After that, the mixture was magnetically separated and the liquid supernatant removed. The microspheres were re-dispersed in 1000 μL of PBS solution, shaken at room temperature for 5 min, and then again separated and re-dispersed using 1000 μL of

PBS solution. This step was repeated 8 times. After which, no HRP molecules were found to have been retained in the liquid supernatant. Finally, we obtained 500 μL of HRP@Microsphere solution, which was then stored at 4 ºC for further use.

200 μL of the HRP@Microsphere solution was magnetically separated and re-dispersed using 200 μL of redistilled water. 10 μL of 20 mg/mL 1-Ethyl-3-(3dimethylaminopropyl) carbodiimide (EDC) solution and 10 μL of 10 mg/mL N-hydroxysuccinimide (NHS) solution were added and the mixture gently shaken at room temperature for 10 min, after which the mixture was magnetically separated and re-dispersed using 200 μL of PBS solution (pH=7.4, 0.01 M). Then, 0.1 mg of antibody (Ab) for MC-LR was added to the mixture which was shaken at room temperature for 1 h. This mixture was magnetically separated, re-dispersed using PBS solution, shaken for 1 min, then separated and the liquid supernatant removed. The remaining HRP@Microspheres@Ab conjugated solids were then re-dispersed using PBS solution. These magnetic separation and washing steps were repeated 3 times. Finally, the MPs-ELISA conjugated product was stored at 4 ºC for further use.

2.3 Characterization of reagents and analytical instruments

All chemical reagents were obtained from Sinopharm Group Co. Ltd. (China). *Chlorella pyrenoidosa* powder was purchased from Qindao Kehai Biochemistry Co. Ltd. (China). Transmission electron microscope (TEM) microphotographs were obtained with a H-7500 instrument (Hitachi, Japan) operating at 80 kV. Field-emission scanning electron microscopy (FESEM) microphotograph was obtained with a SU8020 SEM (Hitachi, Japan) at 2.0 kV. High resolution transmission

electron microscope (HRTEM) images and energy-dispersive X-ray (EDX) spectra were recorded using a JEM-2100F instrument (JEOL, Japan) with an acceleration voltage of 200 kV. N_2 adsorption/desorption isotherms at 77 K were measured using a Micromeritics ASAP 2020 porosity analyser. All samples were degassed under vacuum at 110 ºC for at least 24 h prior to measurement. The pore size distribution of microspheres was obtained from the desorption branch of the isotherms by the BJH (Barrett-Joyner-Halenda) method. The elemental content of samples was determined using an ARL Perform' X 4200 X-ray fluorescence (XRF) analyzer (Thermo-Fisher, USA). Powder X-ray diffraction (XRD) analysis was performed on an X'Pert Pro MPD X-ray diffractometer (Philips, The Netherlands) with Cu-Kα radiation at 40 kV and 40 mA with a scanning rate of 5° min^{-1}. Fourier transform infrared (FTIR) spectroscopy was carried out using a Nicolet 8700 (Thermo-Fisher, USA) Fourier FTIR spectrometer scanning over 500–4000 cm^{-1} at a resolution of 4 cm^{-1}. X-ray photoelectron spectroscopy (XPS) data was collected using an ESCALAB 250Xi (Thermo Scientific, USA), equipped with a monochromatic Al Kα radiation source (1486.6 eV). An multi-mode reader (Synergy HTX; BioTek Instruments Inc., Vermont, USA) was used to obtain absorbance values (OD_{450}). ELISA samples were coated into 96-well PCR plates (Corning Inc. New York, USA). A SuperMag separator was provided by Ocean nanotechnology (USA) to magnetically separate microspheres from liquid supernatant. The MS3 vortex oscillator, used to mix the microspheres and targets, was obtained from IKA -Werke GmbH & Co. KG (Germany).

2.4 Determination of Fe (Ⅱ) and Fe (Ⅲ)

The quantitative assay of Fe (Ⅱ) and Fe (Ⅲ) in the samples were based on standard phenanthroline spectrophotometry [44].

2.5 Analysis of reducing sugars

The determination of reducing sugars in aqueou s phase products was based on 3,5-dinitrosalicylic acid (DNS) spectrophotometry [45].

2.6 Process of MPs-ELISA for detection of MC-LR

100 μL of 50 μg/mL BSA-MC-LR conjugate was coated onto the surface of 96 wells of ELISA plates at 4 ºC for 12 h. After three times washing with PBST (0.01 M PBS, with 0.5% Tween-20), these plates were blocked with blocking buffer (3 wt % BSA in PBS) for 2 h at 37 ºC. After that, 100 μL of MPs-ELISA conjugation was added to 500 μL of samples or MC-LR solution for 30 min. After magnetic separation, 100 μL of PBS was used to re-disperse the MPs-ELISA conjugation product. It was then added to 96-well plates which were then lightly vortexed at 37 ºC for 1 h. The nonspecific adsorption of MPs-ELISA conjugation was then removed and washed 3 times with PBST solution. After that, 50 μL of 3,3',5,5'-tetramethylbenzidine (TMB) was transferred into each well for 5 min at 37 ºC in the dark, after which 50 μL of H_2SO_4 (0.01M) was added into the 96-well plates to halt this reaction. Finally, OD_{450} data was obtained using the BioTek Synergy HTX multi-mode reader.

2.7 Process of conventional ELISA for detection of MC-LR

100 μL of 50 μg/mL BSA-MC-LR conjugate was coated on the surface of 96 wells of ELISA plates at 4 ºC for 12 h. After washing three times with PBST (0.01 M PBS, with 0.5% Tween-20), the plates were blocked with blocking buffer (3 wt % BSA in

PBS) for 2 h at 37 ºC. Then, 100 µL of HRP-Ab conjugate and 100 µL of samples or MC-LR solution were added into the 96-well plates and the plates incubated at 37 ºC for 2 h. After 4 washing steps with PBST solution, 50 µL of TMB was transferred into each well for 5 min at 37 ºC in the dark, after which H_2SO_4 (0.01M; 50 µL) was added to halt this reaction. Finally, OD_{450} data was obtained using the multi-mode reader.

2.8 Water samples analysis

Drinking water samples (designated Samples 1 to 7) were purchased from a local supermarket (Beijing, China). Sample 1 and 2 were employed as blank samples, Sample 3 to 7 were spiked with a series of concentrations of MC-LR. These spiked water samples were used to study the recoveries of MPs-ELISA and conventional ELISA for detection of MC-LR. Sample 8 to 22 were river water samples from a local river (TongHui) in Beijing (China). ELISA was also used to detect MC-LR in these water samples. Each sample was assayed 3 times.

2.9 Loading capacity of HRP by microspheres

400 µL of 4 mg/mL HRP was added to 3.6 mL PBS solution (pH=7.4, 0.01 M) containing 1.26 mg/mL microspheres (pH 10, 200 ºC) and the mixture shaken for 2 h. Afterwards, the mixture was magnetically separated and the supernatant liquid used for determination of the concentration of HRP. Meanwhile, a control without the addition of microsphere and a treatment with microspheres (pH 10, 200 ºC) without cores (obtained by dispersing microspheres (pH 10, 200 ºC) in pH 1 HCl solution for 12 h) were carried out using the same procedure. The concentrations of HRP were

239 determined by spectrophotometry at 403 nm, and the loading capacity of HRP was
240 calculated based on the subtraction method.

241 **3.0 Data analysis and statistics**

242 Unless stated otherwise, all laboratory measurements were performed in triplicate.
243 The error bars in figures indicate standard deviations, which were calculated using
244 MS-Excel.

245 3. Results and Discussion

246 3.1 Structural characterization of rattle-type microspheres

247 **Figure 1A** shows a transmission electron microscope (TEM) image of a raw
248 *Chlorella pyrenoidosa* cell in which the microalgal cell presents a solid spherical
249 structure. After the microalgae were hydrothermally treated at 100 ^{o}C (initial pH 14),
250 hollow structured microspheres were obtained with many nanoparticles inside the
251 microspheres (Figure 1D). When the hydrothermal temperature was increased to 200
252 ^{o}C and the initial pH decreased from 14 to 10 or to 5, not only the spherical hollow
253 shells were maintained at the higher temperature (Figure 1G and J), but also some
254 pores were observed in the shell of the microspheres by field emission scanning
255 electron microscopy (FESEM) (Figure 1E, H and K). In comparison, such obvious
256 pores could not be found in the shell of the raw microalgae (Figure B and C). N_2
257 adsorption/desorption isotherms and pore size distributions of the microspheres at
258 various reaction conditions are detailed in Figure S1. Except for the microspheres (pH
259 14, 100 ^{o}C), the N_2 sorption isotherms of the other microspheres displayed hysteresis
260 loops, which is the characteristic of mesoporous material. The hysteresis loops of the

microspheres (pH 5, 200 ºC) shifted to higher relative pressure, implying an enlargement in pore size during the treatment process [46]. Data calculated using the BJH (Barrett-Joyner-Halenda) method revealed that the most probable pore-size of the microspheres increased from 19.4 nm to 29.7 nm as the hydrothermal temperature was increased from 100 ºC to 200 ºC, and further increased to 46.3 nm when the initial pH of hydrothermal reaction decreased from 10 to 5 at 200 ºC (Figure S1). These results are consistent with those features observed in the FESEM images (Figure 1F, I and L). Additionally, the numbers of nanoparticles significantly decreased with increasing pore-size of the shell (Figure 1J). Although the reasons may be complex, one of the more likely explanations could be that the nanoparticles may readily escape from the shells with bigger pores. Therefore, precisely controlling the pore-size of the shell is both important and necessary in order to find a balance between facilitating mass-exchange and preventing leakage from the cores.

During the fabrication processes, we found that the microspheres (pH 10, 200 ºC) could be separated by an external magnetic field (inset in Figure 1G). However, microspheres (pH 14, 100 ºC) and (pH 5, 200 ºC) did not show this phenomenon (inserts in Figure 1D and J). Interestingly, no other chemical reagents were added during hydrothermal treatment of microalgal biomass, the only differences being in initial pH and reaction temperature. Therefore, the chemical compositions of the microspheres were studied.

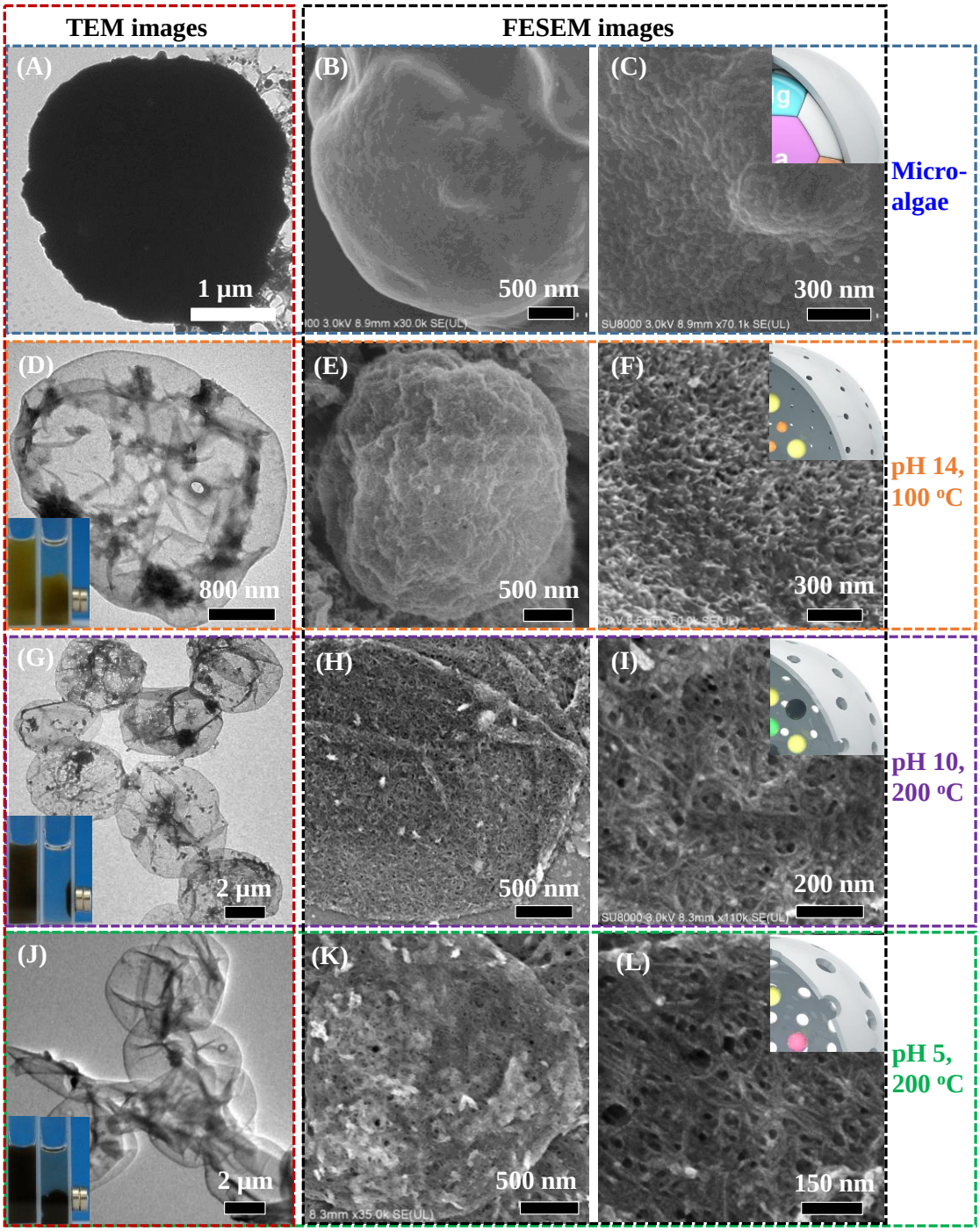

Figure 1. Morphological features of the samples. (A-L) are FESEM and TEM images; the insets in (D, G, and J) are the photos of the response of the microspheres to an external magnetic field; the insets in (F, I, and L) are schematic structures of the shell.

3.2 Chemical characterization of rattle-type microspheres

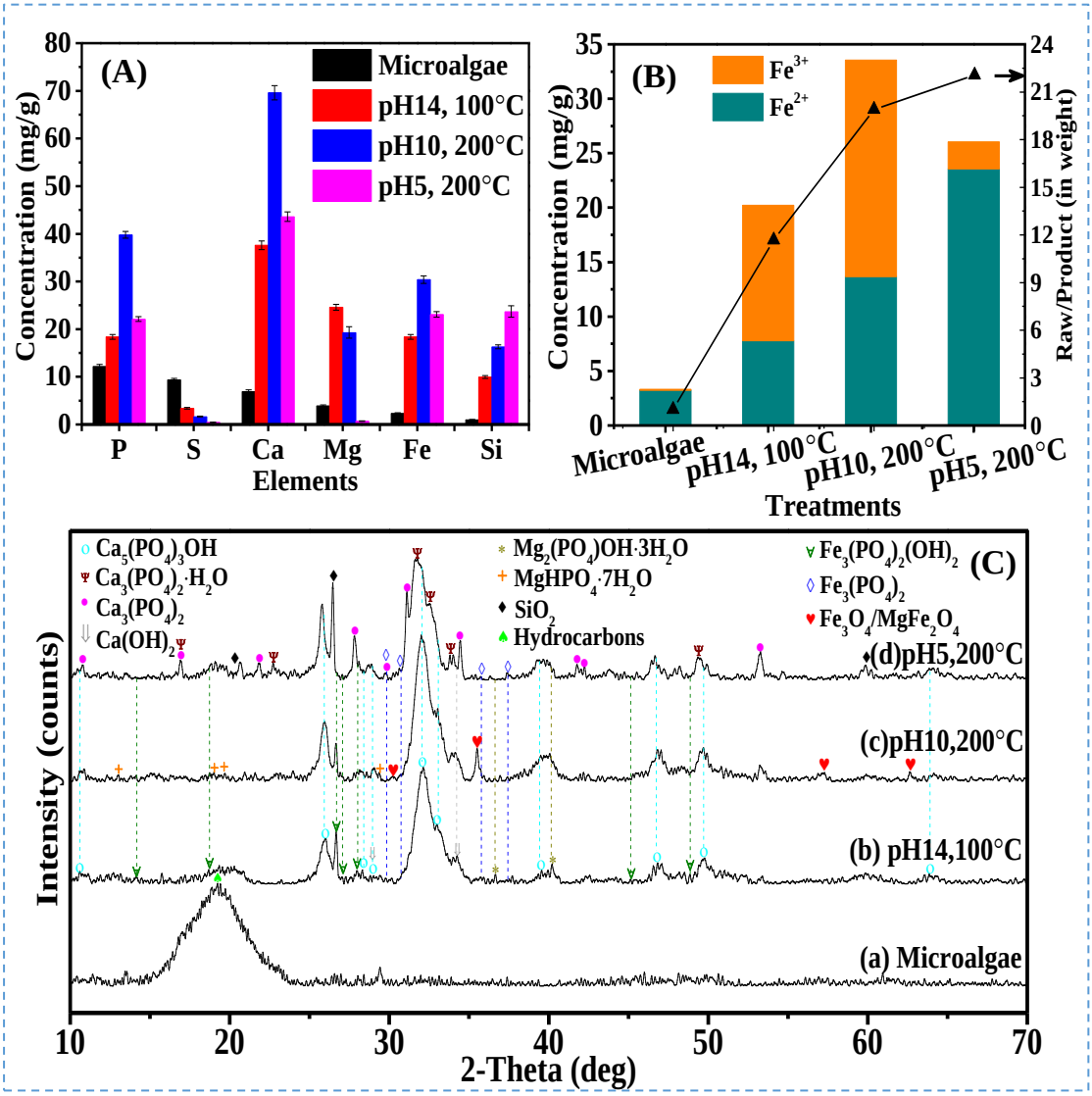

Figure 2. Chemical compositions of the rattle-type microspheres. (A) data from XRF analyses; (B) content of Fe^{2+} and Fe^{3+} in the microspheres and the ratio of raw algae to product under various pH and temperature conditions; (C) XRD spectra from raw algae (a) and products obtained at different pH (b-d).

X-ray fluorescence (XRF) analysis (**Figure 2A)** indicated that the primary inorganic elements of the treated samples were Ca Mg, P, S, Fe and Si, which were all derived from the microalgal biomass. Except for S, the contents of Ca, Mg, P, Fe and Si increased significantly after the raw microalgae were treated under different reaction conditions. From Figure 2B, the weight ratio of raw microalgae to

296 microspheres clearly increased following hydrothermal treatment. We hypothesize
297 that most of the intracellular materials were extracted by the initial treatment with hot
298 alkaline aqueous solution, including S, the main element coming from protein. The
299 elements Ca, Mg, P, Fe and Si may have formed insoluble materials that were trapped
300 inside the cell wall and resulted in the significant increase in the relative contents of
301 these elements by concentration. In order to prove this hypothesis, analysis by X-ray
302 diffraction (XRD) was conducted. Figure 2C-(a) indicates that the broad peak
303 observed between 15-25° refers to hydrocarbon [47], and that no distinct diffraction
304 peaks indicative of the presence of an inorganic phase can be identified from the
305 microalgae biomass. However, after the microalgae were treated with hot solution
306 (100 ºC) at pH 14, $Ca_5(PO_4)_3OH$ was found to be the dominant phase in the
307 microsphere (Figure 2C-(b)). When the temperature was increased from 100 to 200 ºC,
308 several new phases at positions of 30.2°, 35.5°, 47.2°, 57.1° and 62.6° were detected,
309 corresponding to (220), (311), (511), and (440) planes of Fe_3O_4 (PDF card:
310 #19-0629)/$MgFe_2O_4$ (PDF card: #17-0464), respectively, which were present in the
311 microsphere (pH 10, 200 ºC) (Figure 2C-(c)). Moreover, Figure 2B shows that Fe^{3+}
312 and Fe^{2+} were both detected in microsphere (pH 10, 200 ºC). The diffractograms of
313 $MgFe_2O_4$ and Fe_3O_4 are very similar and these compounds are members of spinel
314 ferrite family, which can be best represented as MFe_2O_4 (M=Mg^{2+}, Fe^{2+}) [48], and
315 that Fe_3O_4 and $MgFe_2O_4$, can coexist [49]. As the pH decreased to 5 at 200 ºC,
316 MFe_2O_4 was not be observed in the microsphere (pH 5, 200 ºC) in comparison with
317 the microsphere at pH 10 and 200 ºC (Figure 2C).

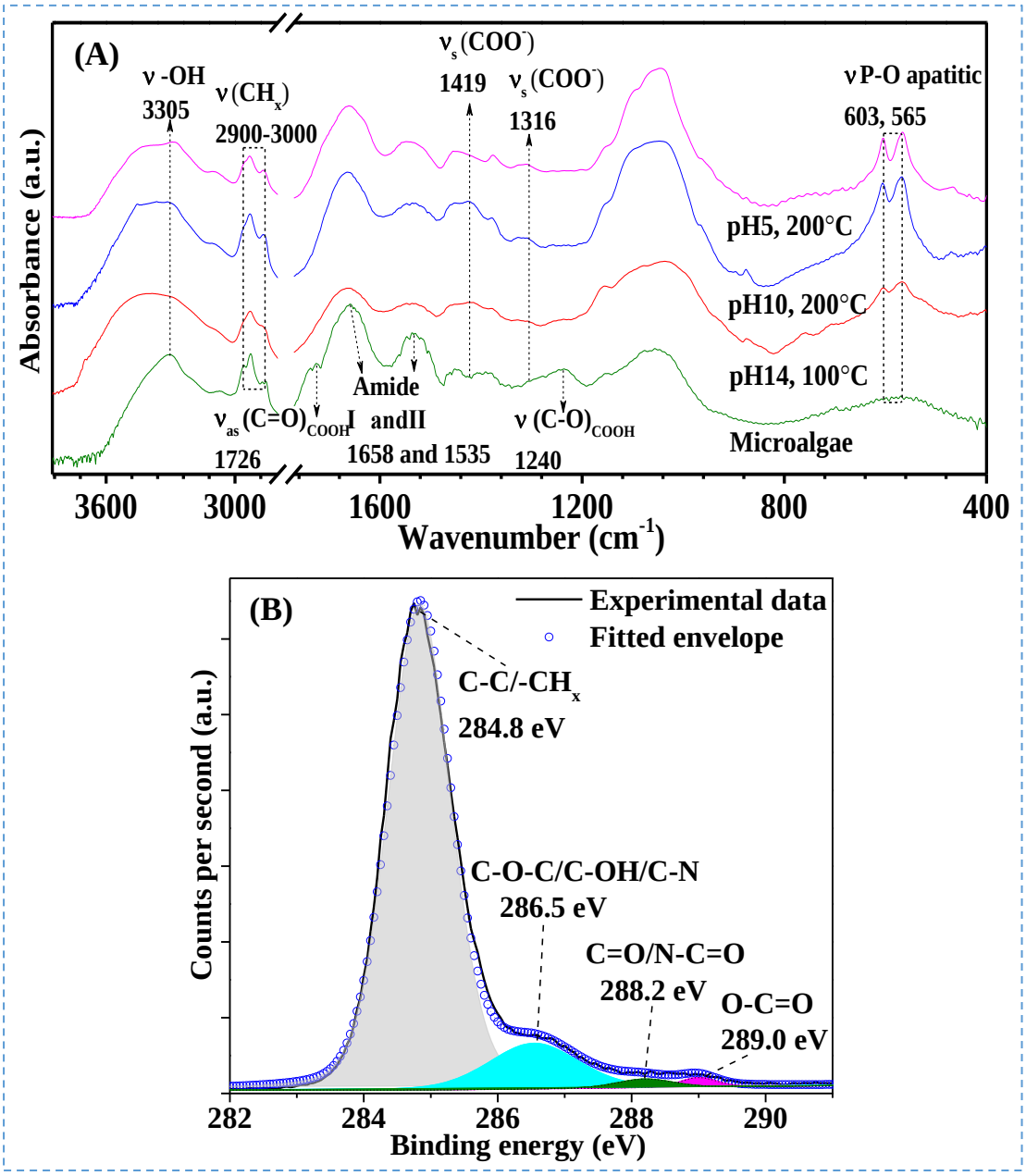

318

319 **Figure 3.** Chemical functional groups of the rattle-type microspheres. (A) is the FTIR

320 spectra. (B) is the high-resolution XPS spectrum in C1s region of microsphere (pH 10,

321 200 °C).

322 Fourier transform infrared (FTIR) spectrum (Figure 3A) suggested that new bands

323 O-P-O had been found in all three treated microspheres, which could be assigned to

324 the PO_4^{3-} formed by the mineralization of organic compounds containing phosphorus

325 inside the microalgae [27], which further confirms the formation of phosphate

minerals in the microspheres. Moreover, the characteristic bands of carboxyl (-COOH) were detected from the raw microalgae. Meanwhile, the bands of carboxylate (COO^-) [50] appeared in microspheres formed at pH 14 and 100 °C and at pH 10 and 200 °C. X-ray photoelectron spectroscopy (XPS) analysis of the C_{1s} region in Figure 3B also proved the existence of [O=C-O (carboxyl)] [51] on the shell. Thus, based on the results of FTIR and XPS, it is hypothesized that a part of the R-COOH derived from microalgae was deprotonated into $R\text{-}COO^-$ under alkaline conditions, and which was preserved in the rattle-type microspheres during the treatment process.

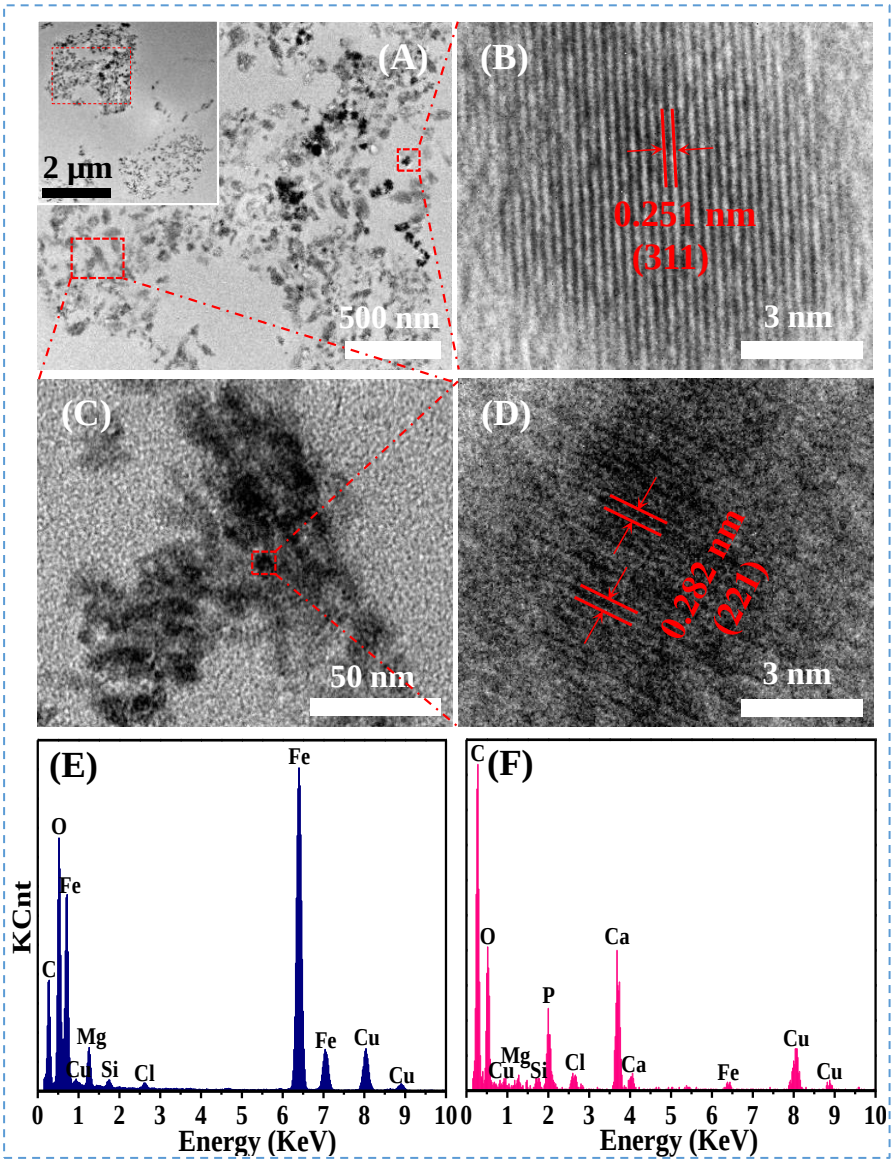

Figure 4. Chemical compositions of the nano-cores in the rattle-type microspheres (pH 10, 200 °C). (A) is a HRTEM image of an ultrathin section obtained from microsphere (pH 10, 200 °C); the inset in (A) is lower magnification HRTEM image of the ultrathin section; (B), (C) and (D) are HRTEM images of the nano cores inside microsphere (pH 10, 200 °C); (E) and (F) illustrate typical spectra obtained from EDX analysis.

To further clarify the exact composition of the nano-cores inside the microspheres (pH 10, 200 °C) which possess magnetic properties, the microspheres were sectioned by ultramicrotome and analyzed by high resolution transmission electron microscopy (HRTEM) and energy dispersive X-ray spectroscopy (EDX). The cores (Figure 4A) were observed to mainly consist of two kinds of nanoparticles: dark-coloured nanoclusters (Figure 4B) and light-colored, needle/sheet-shaped nanoparticles (Figure 4C). Fe, Mg, and O were the dominant elements in the dark-coloured nanoclusters (Figure 4E). Clear lattice fringes could be observed from the dark-colored nanoclusters (Figure 4B), the characteristic interplanar distance of 0.251 nm matching well with the d-spacing of the crystalline plane (311) of $MgFe_2O_4/Fe_3O_4$ [52, 53]. Thus, based on the results of XRF, XRD, EDX and HRTEM, the dark-coloured nano clusters were found to be mainly composed of Fe_3O_4 and $MgFe_2O_4$, which is the reason that the microspheres (pH 10, 200 °C) possessed magnetic properties. Additionally, Figure 4 F indicates that Ca, P and O were the dominant elements of the light-colored, needle/sheet-shaped nanoparticles. The mass ratio of Ca to P was determined to be 2.11 correlating well with the mass ratio of Ca/P=2.15 in

$Ca_5(PO_4)_3OH$ (Table S1). Meanwhile, the HRTEM image in figure 4D reveals that the fringes in the light-colored, needle/sheet-shaped nanoparticles were not distinct and intact, implying poor crystallinity. The lattice fringe with a spacing distance of 0.282 nm is in a good agreement with the (221) plane of $Ca_5(PO_4)_3OH$, which is consistent with the results of the XRD analysis. Therefore, it is reasoned that $Ca_5(PO_4)_3OH$ was the main component of the light-colored needle/sheet-shaped nano particles.

3.3 Formation mechanism of the microalgae-derived microspheres

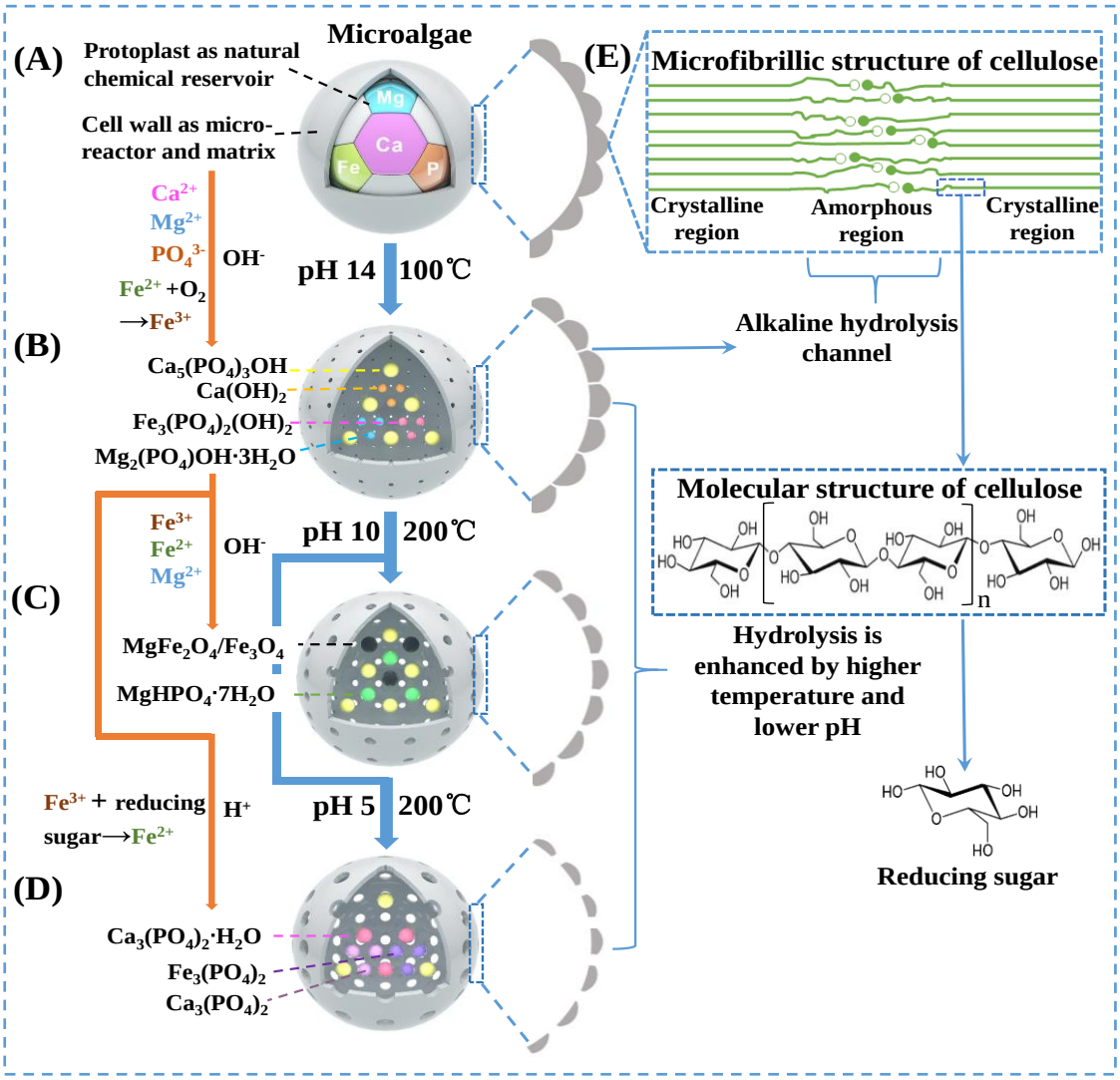

Scheme 2. Proposed mechanism of formation of the microalgae-derived rattle-type microspheres with simultaneous controllable multicomponent nano-cores and porous

shells.

With reference to the preceding results, the mechanism of formation of the microalgae-derived rattle-type microspheres is depicted in **Scheme 2.** The protoplast of the microalgae (Scheme 2A) acted as a natural chemical reservoir of Ca, Si, Mg, P and Fe, which formed insoluble nano-cores of metal phosphates and were trapped inside the cell wall when treated at high pH (pH=14). Meanwhile, most of the intracellular materials were extracted by the hot aqueous alkaline solution, leading to the formation of a rattle-type structure (Scheme 2B). When the temperature increased (100 to 200 °C) and the pH decreased (14 to 10), the solubility of metal phosphates was raised, resulting in the release of Fe^{2+}, Mg^{2+} and Fe^{3+}, forming magnetic nano-cores ($MgFe_2O_4/Fe_3O_4$) under medium pH conditions (pH=10) (Scheme 2C). As the pH decreased from 14 to 5, most of the Fe^{3+} was reduced to Fe^{2+} by the reducing sugars present (**Figure S2**), blocking the formation of magnetic materials under these conditions (Scheme 2D).

Cellulose, as the primarily component of cell walls in *Chlorella pyrenoidosa* [54], is composed of microfibrils which have both crystalline and amorphous regions (Scheme 2E). Under high pH conditions (pH>12), alkaline degradation takes place in the amorphous regions of cellulose through peeling-off reaction [55], forming alkaline hydrolysis channels in the cell wall. As the pH decreased and the temperature raised, the hydrolysis of cellulose was significantly increased, enhancing reducing sugar formation (Figure S2), leading to continued enlargement of these hydrolysis channels. Therefore, the pore-sizes of the shell can be tuned by adjusting only the initial pH and

hydrothermal temperature.

3.4 Analytical performance of immunosensors based on rattle-type microspheres (pH 10, 200 ºC).

The microalgae-derived rattle-type microspheres present some potential advantages as signal multipliers for immunoassay. Firstly, the hollow and porous structure is an attractive carrier to load enzymes for construction of an immunosensor. Secondly, the existence of natural COO^- on the shell would facilitates subsequent bio-conjugation of antibodies with no need for complex surface functionalization. Lastly, the multicomponent cores may be beneficial for the loading of enzymes and for magnetic separation. Hence, in a subsequent study, we attempted to construct an immunosensor using microsphere (pH 10, 200 ºC) as signal multipliers in horseradish peroxidase (HRP)@Microspheres@Antibody(Ab)-mediated ELISA (MPs-ELISA) for the detection of microcystin-LR (MC-LR) based on competitive immunoassay and useing conventional ELISA for comparison **(Figure 5A)**.

The OD_{450} value in MPs-ELISA decreased when the concentration of MC-LR increased from 0.01 ng/mL to 1000 ng/mL (Figure 5B). The linear range of MPs-ELISA for detection of MC-LR is 0.05 ng/mL to 100 ng/mL, and the limit of quantification (LOQ) is 0.05 ng/mL. The linear equation is Y=-0.26X+0.75 (X=lg[MC-LR(ng/mL)], R^2=0.97) (Figure 5D). In conventional ELISA, the OD_{450} value decreased when the concentration of MC-LR increased from 0.05 ng/mL to 1000 ng/mL (Figure 5C). The linear range of this conventional ELISA for detection of MC-LR is 0.5 ng/mL to 50 ng/mL, and the LOQ is 0.5 ng/mL. The linear equation is

Y=-0.26X+0.67 (X=lg[MC-LR (ng/mL)], R^2=0.96) (Figure 5E). Therefore, the sensitivity (LOQ) and the linear range of MPs-ELISA demonstrated an improvement by about an order of magnitude when compared with conventional ELISA.

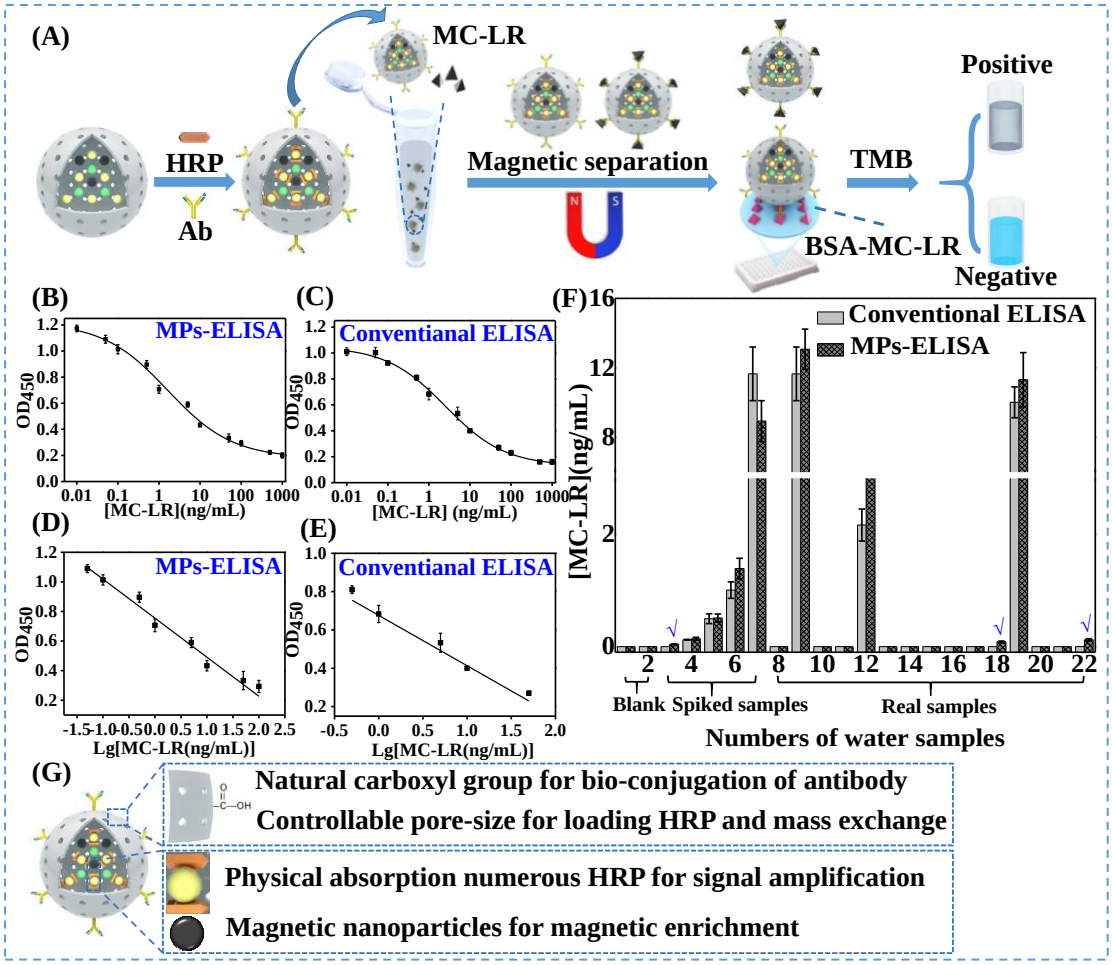

Figure 5. Analytical performance of MPs-ELISA and conventional ELISA for detection of MC-LR. (A) is the process of MPs-ELISA for detection of MC-LR; (B) and (C) are the standard curves of MPs-ELISA and conventional ELISA for detection of MC-LR; (D) and (E) are the linear range of MPs-ELISA and conventional ELISA for MC-LR detection (the concentration of MC-LR ranging from 0.05 to 100 ng/mL); (F) is the results of MPs-ELISA and conventional ELISA for detection of MC-LR in spiked water samples and real water samples. The real water samples were collected

422 from three local rivers in Beijing (China). The blue √ indicates the water samples have
423 tested positive. (G) Illustration of the mechanisms of improvement on analytical
424 sensitivity by microspheres.

425 Conventional ELISA and MPs-ELISA were also employed to detect MC-LR in
426 spiked and real water samples (Figure 5F). Sample 3 to 7 were spiked samples, with
427 concentrations from 0.05 ng/mL to 10 ng/mL. Sample 3 was detected to be MC-LR
428 negative by conventional ELISA; in contrast, it was detected to be MC-LR positive by
429 MPs-ELISA, with a detected concentration of 0.04 ng/mL. The reason for this finding
430 was that the LOQ of conventional ELISA for detection of MC-LR was 0.5 ng/mL,
431 while the LOQ of MPs-ELISA for detection of MC-LR was 0.05 ng/mL. For real
432 water samples (samples 8-22), sample 18 and 22 were detected to be MC-LR negative
433 by conventional ELISA, because the concentration of MC-LR in these two samples
434 were low and the sensitivity of conventional ELISA could not satisfy the detectability
435 requirement. However, the improved sensitivity of MPs-ELISA enabled this technique
436 to detect traces of MC-LR in real water samples.

437 This enhancement for the sensitivity can be concluded from the following reasons
438 (Figure 5G): 1) the nanocores of $Ca_5(PO_4)_3OH$ have high affinity for enzymes[56] and
439 provide many more active sites for the anchoring of HRP compared with the
440 microspheres without cores **(Figure S3-A)**; 2) as HRP was physically adsorbed on the
441 cores, there was little effect on HRP activity, but conversely, there would be an loss in
442 activity of about 15% if it was covalently conjugated to commercial magnetic
443 nanoparticles (MNPs) (Figure S3-(B)); 3) the magnetic responsiveness of the

microspheres realizes immunomagnetic separation and enrichment. In this assay, the sample enrichment factor is 5, which is one of the main reasons for the enhancement of the sensitivity of MPs-ELISA. In addition, compared with commercialized MNPs, the rattle-type microspheres are less expensive and do not need any surface modification and functionalization due to the existence of natural carboxyl groups on the shell, which contribute to make the immunoassay simpler and less costly.

4. Conclusion

In summary, a simple and environmentally friendly route to produce rattle-type microspheres with simultaneous controllable multicomponent cores and porous shells using microalgae as the single-source precursor, has been successfully developed. Specifically, the unique structural and chemical characteristics of the microalgae-derived rattle-type microspheres can not only load large amounts of enzyme and retain its activity without covalent conjugation, but also can achieve magnetic enrichment and bioconjugation with antibodies without surface functionalization. These properties can significantly improve sensitivity and simplify conventional ELISA. Additionally, the rattle-type microspheres with tuneable pore-size shells are natural separators, which may be used to sieve and augment virus or nanoparticles of different sizes. Meanwhile, the multicomponent cores, containing moieties such as Fe_3O_4, $MgFe_2O_4$, and $Ca_5(PO_4)_3OH$, could act as magnetic resonance imaging probes, nonenzyme or adsorbent, which are the areas where further work will be focused. In conclusion, the advanced microalgae-derived rattle-type microspheres is a flexible platform which has the potential to find wide application in biosensors,

drug delivery, enrichment and separation of target substances, and environmental remediation.

Supporting Information

Supporting Information is available from the author.

Author information

Corresponding Authors

E-mail: chenyiping@mail.hzau.edu.cn

E-mail: gpan@rcees.ac.cn

Notes

The authors declare no competing financial interest.

Acknowledgements

This study was supported by the National Key R&D Program of China (2017YFA0207204), the National Natural Science Foundation of China (Grant No. 21806175 and 81671784), and the Medical Technologies and Advanced Materials Strategic Theme at Nottingham Trent University,UK We thank Doctor De-zhi Ni for the constructive suggestion of the results. We thank Mick Cooper for proof reading.

References

[1] Okamoto, M.; Tsukada, H.; Fukasawa, S.; Sakajiri, A. *J. Mater. Chem. A* **2015**, *3*, 11880.

[2] Jiao, Y.; Sun, Y.; Tang, X.; Ren, Q.; Yang, W. *Small* **2015**, *11*, 1962.

[3] S.S. Said, S. Campbell, T. Hoare, Externally Addressable Smart Drug Delivery Vehicles: Current Technologies and Future Directions, Chem. Mater. **2019,** 4971-4989.

[4] M. Karg, A. Pich, T. Hellweg, T. Hoare, L.A. Lyon, J.J. Crassous, D. Suzuki, R.A. Gumerov, S. Schneider, I.I. Potemkin, Langmuir **2019,** 6231-6255.

[5] Wu, Z. C.; Li, W. P.; Luo, C. H.; Su, C. H.; Yeh, C. S. *Adv. Funct. Mater.* **2015**, *25*, 6527.

[6] Tsai, M. F.; Hsu, C.; Yeh, C. S.; Hsiao, Y. J.; Su, C. H.; Wang, L. F., *ACS appl. Mater. Inter.* **2018,** *10* (2), 1508-1519.

[7] Kalantari, M.; Yu, M.; Noonan, O.; Song, H.; Xu, C.; Huang, X.; Xiang, F.; Wang, X.; Yu, C.

Chemosphere **2017**, *166*, 109.
[8] J.-P. Fan,; J.-X. Yu,; X.-M. Yang,; X.-H. Zhang,; T.-T. Yuan,; H.-L. Peng., *Chem. Eng. J.* **2018**, *337,* 722-732.
[9] Yue, Q.; Li, J.; Zhang, Y.; Cheng, X.; Chen, X.; Pan, P.; Su, J.; Elzatahry, A. A.; Alghamdi, A.; Deng, Y.; Zhao, D. *J. Am. Chem. Soc.* **2017**, *139*, 15486.
[10] Li, X.; Zheng, W.; Chen, B.; Wang, L.; He, G. *ACS Sustain. Chem. Eng.* **2016**, *4*, 2780.
[11] S. Zhang, H. Gao, X. Xu, R. Cao, H. Yang, X. Xu, J. Li, *Chem. Eng. J.* **2020**, *381*, 122670.
[12] Y. Zhuang, S. Yuan, J. Liu, Y. Zhang, H. Du, C. Wu, P. Zhao, H. Chen, Y. Pei, *Chem. Eng. J.* **2020**, *379*, 122262.
[13] L. Wang, X. Yu, X. Li, J. Zhang, M. Wang, R. Che, *Chem. Eng. J.* **2020**, *383*, 123099.
[14] Zhou, L.; Zhuang, Z.; Zhao, H.; Lin, M.; Zhao, D.; Mai, L. *Adv. Mater.* **2017**, *29,* 1602914.
[15] W. Gou, X. Kong, Y. Wang, Y. Ai, S. Liang, A. Pan, G. Cao, *Chem. Eng. J.* **2019**, *374*, 545-553.
[16] H. Kim, D. Kim, Y. Lee, D. Byun, H.-S. Kim, W. Choi, *Chem. Eng. J.* **2020**, *383*, 123094.
[17] Qiao, Z. A.; Huo, Q.; Chi, M.; Veith, G. M.; Binder, A. J.; Dai, S. *Adv. Mater.* **2012**, *24*, 6017.
[18] Li, J.; Song, S.; Long, Y.; Yao, S.; Ge, X.; Wu, L.; Zhang, Y.; Wang, X.; Yang, X.; Zhang, H. *Chem. Sci.* **2018**. *9,* 7569.
[19] W. Zhu, Z. Chen, Y. Pan, R. Dai, Y. Wu, Z. Zhuang, D. Wang, Q. Peng, C. Chen, Y. Li, *Adv Mater* **2018** e1800426.
[20] Li, B.; Zeng, H. C. *Adv. Mater.* **2018**, 1801104.
[21] Mata, T. M.; Martins, A. A.; Caetano, N. S. *Renew. Sust. Energ. Rev.* **2010**, *14*, 217
[22] Liu, J.; Yang, T.; Wang, D.-W.; Lu, G. Q. M.; Zhao, D.; Qiao, S. Z. *Nat. commun.* **2013**, *4*, 2798.
[23] L. Zhang, X. Liu, Y. Dou, B. Zhang, H. Yang, S. Dou, H. Liu, Y. Huang and X. Hu, *Angewandte Chemie*, 2017, **56**, 13790-13794.
[24] Zhong, Y.; Xia, X.; Deng, S.; Xie, D.; Shen, S.; Zhang, K.; Guo, W.; Wang, X.; Tu, J. *Adv. Mater.* **2018**, 1805165.
[25] Sun, L.; Zhang, D.; Sun, Y.; Wang, S.; Cai, J. *Adv. Funct. Mater.* **2018**, *28*, 1707231.
[26] He, W.; Min, D.; Zhang, X.; Zhang, Y.; Bi, Z.; Yue, Y. *Adv. Funct. Mater.* **2014**, *24*, 2206.
[27] Bi, L.; Pan, G. *Sci. Rep.* **2017**, *7*, 15477.
[28] Bi, L.; Pan, G. *J. Mater. Chem. A* **2014**, *2*, 3715.
[29] D. Ni, L. Wang, Y. Sun, Z. Guan, S. Yang and K. Zhou, *Angewandte Chemie*, **2010**, *49*, 4223-4227.
[30] Z. Zeng, Y. Zhong, H. Yang, R. Fei, R. Zhou, R. Luque and Y. Hu, *Green Chem*, **2016**, *18*, 186-196.
[31] F. Bella, J.R. Nair, C. Gerbaldi, RSC advances, **2013**, *3*, 15993-16001.
[32] L. Fagiolari, F. Bella, *Energ. Environ. Sci.*, **2019**, *12*, 3437-3472.
[33] P. Sennu, V. Aravindan, Y.-S. Lee, *Chem. Eng. J.* **2017**, *324*, 26-34.
[34] P. Avetta, F. Bella, A. Bianco Prevot, E. Laurenti, E. Montoneri, A. Arques, L. Carlos, *ACS Sustain. Chem. Eng.*, **2013**, *1*, 1545-1550.
[35] G. Piana, M. Ricciardi, F. Bella, R. Cucciniello, A. Proto, C. Gerbaldi, *Chem. Eng. J.* **2020**, *382*, 122934.
[36] L. Zolin, J.R. Nair, D. Beneventi, F. Bella, M. Destro, P. Jagdale, I. Cannavaro, A. Tagliaferro, D. Chaussy, F. Geobaldo, *Carbon*, **2016**, *107*, 811-822.
[37] X. Zhang, J. Li, J.-Y. Yang, K.V. Wood, A.P. Rothwell, W. Li, E.R. *Environ. Sci. Tech.*, **2016**, *50*, 7671-7678.

[38] M. Lotierzo, R. Abuknesha, F. Davis, I. Tothill, *Environ. Sci. Tech.*, **2012**, *46*, 5504-5510.
[39] Xianyu, Y.; Wu, J.; Chen, Y.; Zheng, W.; Xie, M.; Jiang, X. *Angew. Chem. Int. Ed.* **2018**, *57*, 7503.
[40] Krishnan, S.; Mani, V.; Wasalathanthri, D.; Kumar, C. V.; Rusling, J. F. *Angew. Chem. Int. Ed.* **2011**, *50*, 1175.
[41] Chen, Y.; Xianyu, Y.; Wang, Y.; Zhang, X.; Cha, R.; Sun, J.; Jiang, X. *ACS nano.* **2015**, *9*, 3184.
[42] Zhu, N.; Ji, H.; Yu, P.; Niu, J.; Farooq, M. U.; Akram, M. W.; Udego, I. O.; Li, H.; Niu, X. *Nanomaterials* **2018**, *8*.
[43] Liu, J.; Qiao, S. Z.; Chen, J. S.; Lou, X. W.; Xing, X.; Lu, G. Q. *Chem. Commun.* **2011**, *47*, 12578.
[44] Stucki, J. W. *Soil Sci. Soc. Am. J.* **1981,** 638-641.
[45] Gusakov, A. V.; Kondratyeva, E. G.; Sinitsyn, A. P.; *Int. J. Anal. Chem.* **2011,** *4***,** 283658**.**
[46] L. Cao, D. Chen, W.-Q. Wu, J.Z. Tan, R.A. Caruso, *J. Mater. Chem. A*, **2017**, *5*, 3645-3654.
[47] Kang, S.; Li, X.; Fan, J.; Chang, J. *Ind. Eng. Chem. Res.* **2012**, *51*, 9023.
[48] Ilhan, S.; Izotova, S. G.; Komlev, A. A. *Ceram. Int.* **2015**, *41*, 577.
[49] Keny, S. J.; Manjanna, J.; Venkateswaran, G.; Kameswaran, R. *Corros. Sci.* **2006**, *48*, 2780.
[50] Mansur, A. A. P.; de Carvalho, F. G.; Mansur, R. L.; Carvalho, S. M.; de Oliveira, L. C.; Mansur, H. S. *Int. J. Biol. Macromol.* **2017**, *96*, 675.
[51] Falco, C.; M. Sevilla, R. J. White, R. Rothe, M. M. Titirici, *ChemSusChem* **2012**, *5*, 1834.
[52] Y. Shen, Y. Wu, X. Li, Q. Zhao, Y. Hou, *Mater. Lett.*, **2013**, *96*, 85-88.
[53] M. Bououdina, B. Al-Najar, L. Falamarzi, J.J. Vijaya, M. Shaikh, S. Bellucci, *Eur. Phys. J. Plus*, **2019**, *134*, 84.
[54] Northcote, D.; Goulding, K.; Horne, R.; *Biochemical Journal* **1958**, *70*, 391.
[55] Wei, J.; *Polymer Degradation and Stability* **2018**, *150*, 1.
[56] Ma, Y.; Zhang, J.; Guo, S.; Shi, J.; Du, W.; Wang, Z.; Ye, L.; Gu, W. *Mat. sci. eng. C-mater.* **2016**, *68*, 551.